Anisotropic behaviour of extruded short carbon fibre reinforced PEEK under static and fatigue loading

Andrea Avanzini[1], Davide Battini[1]*, Candida Petrogalli[1], Stefano Pandini[1], Giorgio Donzella[1]

[1] *Department of Mechanical and Industrial Engineering, University of Brescia, Via Branze 38, 25123 – Brescia, Italy*

*corresponding author, davide.battini@unibs.it

ORCIDs:	Andrea Avanzini	0000-0002-7188-7687
	Davide Battini	0000-0002-2044-5985
	Candida Petrogalli	0000-0002-1774-3914
	Stefano Pandini	0000-0003-2390-8495
	Giorgio Donzella	0000-0002-6972-7035

Cite this article

Avanzini, A., Battini, D., Petrogalli, C. *et al.* Anisotropic Behaviour of Extruded Short Carbon Fibre Reinforced PEEK Under Static and Fatigue Loading. *Appl Compos Mater* (2022). https://doi.org/10.1007/s10443-021-10004-1

Received: 12 August 2021 Accepted: 29 November 2021 Published: 02 February 2022

Citation download link: Download citation

DOI link: Link to the paper via DOI address

Direct link to publisher: Direct link to the paper on Springer's website

Direct shareable link to open-access read-only version: OA Read-Only version

Abstract

The influence of fibre orientation on an extruded short carbon fibre PEEK composite, reinforced with 30% weight fraction of short carbon fibres, was investigated. Specimens were obtained from extruded plates along directions transverse and parallel to the extrusion flow and different types of fibre spatial arrangements were observed. Prior to fatigue testing the elastic modulus of each specimen was measured and the specimens were grouped into homogeneous families, from low to high modulus. Each family exhibited distinct fatigue strength, associated with different progressive damage patterns and failure mechanisms. With increasing alignment of the fibres along the loading axis, a noticeable improvement of fatigue strength could be observed, whereas when the fibres were mostly perpendicular, fatigue properties were even lower than those of unreinforced PEEK. Overall, results suggest that extruded short carbon fibre PEEK products may exhibit a heterogeneous microstructure and a wide range of fatigue properties, making the definition of design allowables a critical task.

Keywords

Carbon fibre; Short fibre reinforcement; Fatigue; Mechanical properties; Anisotropic behaviour; PEEK

Statements and Declaration

Funding: no funds, grants, or other support was received.

Conflict of interests: the authors have no relevant financial or non-financial interests to disclose.

Code availability: not applicable

Availability of data and materials: the raw and the processed data required to reproduce these findings cannot be shared at this time due to technical or time limitations.

Authors' contributions

Conceptualization [Andrea Avanzini]; Methodology [Andrea Avanzini, Davide Battini, Candida Petrogalli, Stefano Pandini]; Investigation [Andrea Avanzini, Davide Battini, Candida Petrogalli, Stefano Pandini, Giorgio Donzella]; Resources [Andrea Avanzini, Candida Petrogalli, Stefano Pandini, Giorgio Donzella]; Writing - Original Draft [Andrea Avanzini]; Writing - Review & Editing [Andrea Avanzini, Davide Battini, Candida Petrogalli, Stefano Pandini, Giorgio Donzella]; Data Curation [Andrea Avanzini, Davide Battini]; Visualization [Andrea Avanzini, Davide Battini, Candida Petrogalli, Stefano Pandini]; Supervision [Andrea Avanzini, Giorgio Donzella]

1. Introduction

Short fibre reinforced (SFR) thermoplastics have been used since a long time in several industrial fields, thanks to the possibility of increasing mechanical properties, in comparison to base polymers, while maintaining the ease of processing and the lower costs traditionally associated with thermoplastics manufacturing processes. For high performance polymers, such as polyetheretherketone (PEEK), the inclusion of short carbon or glass fibres can lead to a remarkable increase of strength, stiffness, and wear properties [1–3]. The combination of excellent mechanical properties with a high continuous service temperature and good chemical resistance in many environments, makes SFR-PEEK particularly suitable for load-bearing structural applications, ranging from the biomedical field to aerospace, oil&gas and mechatronics [4–6]. Many structural applications involve cyclic loading and this motivated investigations on fatigue strength and damage of PEEK and its SFR composites [7–10], as well as on the influence of notches [11–13]. The reinforcing effect of short fibres depends on several factors, including fibre volume fraction, length, adhesion to the matrix, and, of course, fibre material. In general, a high fibre content is required to achieve a high performance SFR-thermoplastic composite, and the mechanical properties such as strength, modulus, and toughness usually increase with an increasing fibre length [14]. However, SFR-thermoplastics are complex materials whose microstructure is set up during the manufacturing process, in particular regarding the spatial arrangement of the fibres and the presence of some preferred orientations for the reinforcing phase, as documented with different methods like image analysis, X-ray CT, in-situ micro-tomography [15–18]. Specimens or industrial components made of the same matrix and reinforcement

phases are likely to exhibit significant differences in microstructure and properties when different processing/manufacturing conditions are met. Various moulding technologies are currently available for the manufacturing of SFR-PEEK, including injection, compression, and extrusion. Recently, 3D printing with FDM is also emerging as an attractive alternative to traditional processes [19]. Most of the published investigations on SFR-thermoplastics deal with injection moulding, both because of its industrial importance and because of the relative ease of manufacturing standardized specimens for mechanical characterization or research purposes. For injection moulded SFR-thermoplastic, the presence of a layered skin-core structure with different preferred fibre orientation is often reported, in which the thickness and preferred layered orientations is dependent on processing conditions (flow speed, viscosity, and temperatures) [16, 20]. Fibre alignment parallel to the moulding flow direction is a rather likely condition in injection moulded specimens for the uniaxial tensile test. In fact, this condition is often referred at by resin manufacturers in terms of datasheet or certified properties. More in general, injection moulding allows a controlled flow condition, which is particularly advantageous to investigate fibre orientation effects by cutting specimens from an injection moulded plate at different angles. When considering fatigue-related aspects, the dependency of fatigue behaviour on fibre orientation has been documented in [21–23] for SFR-thermoplastics polymers such as PPS, PBT and PA6. Moreover, advanced constitutive models for short fibre reinforced thermoplastics were also recently proposed in [24–27]. When considering PEEK specifically, the effects of short fibre reinforcement on fatigue crack propagation were considered in [28] and [29] where an average planar fibre orientation was assumed. The most common alternative to injection moulding is extrusion, by which semi-finished product (plates, rods, tubes) are first obtained and then machined to the final shape of the component. Essentially, extruded products are made by using a die that is shaped in the desired cross-section and by changing the shape of the opening in the die, different extruded shapes are possible. Hollow structures are also manageable if using an inner mandrel. Conventional dies show a common alignment in the direction of the extrusion, both for fibres and polymer chains, but the degree of such alignment depends on the length and width of the restricted flow paths [30]. For example, the fibre orientation can be changed laterally to the machine direction by significantly expanding the flow path. Significant changes in orientation can also be achieved with a change in the geometry of the die or by using an expanding mandrel die, an obstructed die or a combination die, resulting in a transverse or random fibre distribution [26]. Unfortunately, manufacturers do not disclose these processing details and provide little guidance on the expected orientation. Overall, it can be concluded that fibre orientation in an extruded component is difficult to be predicted a priori and that it must be determined by separate testing under individual circumstances. Therefore, in contrast with injection moulded products, predicting the presence of a preferred

fibre orientation is a challenging task when specimens are machined from extruded plates or rods at different positions. Consequently, there is a lack of published investigations on the effect of anisotropy on mechanical and fatigue behaviour of extruded short fibre reinforced thermoplastics, in particular for SFR-PEEK. Based on the above-mentioned considerations, the present research investigates the influence of preferred fibre orientation on fatigue behaviour of an extruded PEEK composite, reinforced with short carbon fibres (a.k.a. PEEK CF30, due to the 30% nominal carbon fibre weight fraction). To this aim, specimens were first obtained from extruded plates by cutting along different directions (i.e., transverse and parallel to the plate edges) at different (random) positions. Prior to fatigue testing, the elastic modulus of each specimen was measured, showing a considerable scatter of observed values. This partially unexpected finding suggested the presence of distinct types of fibre distributions and orientations and provided a unique opportunity to investigate their effect on fatigue strength. To this aim, the specimens were grouped into more homogeneous families from low to high elastic moduli (E) and then subjected to fatigue testing. After the tests, the fibre orientation was analysed on the polished sections of the specimens and the fracture surfaces were also compared. Such investigations revealed a significant influence of fibre orientation on fatigue strength, damage, and failure mechanisms. Methods and results will be discussed in the following paragraphs, along with considerations on the consequences these findings may have on design strategies.

2. Materials and methods

2.1 Material and specimens

Static and fatigue tests were carried out on dogbone shaped specimens obtained from commercially available semifinished extruded plates made of PEEK reinforced with short carbon fibres (weight fraction 30%). A total of 50 specimens were tested: 44 specimens were used for fatigue tests and 6 specimens for static tests. Optical microscope observations of the polished surface along the longitudinal and transverse sections allowed determining fibres dimensions with an average diameter of 7 μm and a length of 0.15 mm. These values represent an estimate, based on a 2D analysis, of the true average fibre dimensions, which should ideally be determined with 3D analysis. Due to manufacturing constraints on the dimensions of the semifinished plates, the plate was cut into 6 mm thick slices, from which dogbone specimens with a 6 mm x10 mm cross-section in the gauge region were then machined. Detailed specimen dimensions and geometry can be found in [7].

The specimens were cut in various positions along two perpendicular directions, parallel to the edges of the plates which should correspond to directions aligned and perpendicular to the extrusion flow. No details on the processing methods and parameters were available and thus, correlations between extrusion parameters and material properties were not attempted, leaving to future work the investigation on the relationship between processing set-up, fibre orientation and mechanical properties. Furthermore, this approach is also driven by real-life designing conditions since in complex shaped parts, as those obtained by machining extruded semifinished products, the actual fibre orientation is a-priori unknown.

2.2 Test protocol

Tensile tests were preliminarily carried out on a total of six specimens sorted from both directions (aligned and transverse) and from different locations on the plate, using a servo-hydraulic testing machine INSTRON 8501. The tests were displacement controlled at a crosshead speed of 0.25 mm/min, with the strain being measured by an extensometer (INSTRON mod. 2620-601, 25 mm gage length), up to failure. The results of this preliminary investigation revealed a significant dispersion of stiffness and strength values, as well as inherently different behaviours in terms of elongation at break and related ductility. Section 3.1 also reports a more detailed discussion of this finding. In addition, based on this evidence, it was decided to systematically measure the elastic modulus of each available specimen prior static or fatigue testing. To this aim, a quasi-static test was carried out in which a ramp load up to 2400 N was applied, while keeping the extensometer mounted. The corresponding strain levels depend on the stiffness of each specimen and ranged approximately between 0.0016 and 0.0072. On average, the resulting strain rate was about 0,0017 s-1. The 2400N value corresponds to an engineering stress of 40 MPa, well within the material elastic range, to avoid damage. Thanks to the extensometer, the elastic modulus E of each sample was in this way accurately determined. The specimens were then categorized based on values of E, independently from the specimen cutting direction, into four families as follows:

- High Modulus (HM): Specimens with E in the range 19000 -24000 MPa
- Intermediate modulus (IM)
    - IHM – (Intermediate High Modulus): Specimens with E in the range 16000 -18000 MPa
    - ILM – (Intermediate Low Modulus): Specimens with E in the range 9000 -13000 MPa
- Low Modulus (LM): Specimens with E in the range 5500-7000 MPa

It should be remarked, as also apparent from Fig.1, that it was not possible to group the specimens into perfectly homogeneous classes, especially for the samples with higher elastic modulus. Fatigue testing was carried out assuming that each different modulus family should be tested within different fatigue load ranges. Although somewhat arbitrary, this preliminary classification proved to be very useful for the correct choice of loading levels and subsequent interpretation of fatigue testing results. Load-controlled tension–tension fatigue tests were performed on a servo-hydraulic testing machine INSTRON 8501. To avoid any surface damage, during fatigue test the extensometer was not used and the evolution of the stiffness was monitored basing on crosshead displacement. The number of cycles to failure was limited to 10^6 and a sinusoidal load cycle was applied. A very small but positive minimum load (lower than 30 N) was always applied to guarantee test stability while achieving a load ratio R = (min. load) / (max. load) ≈ 0. The cyclic frequency was set to 10 Hz. The applied nominal stress was evaluated by dividing the applied load by the reference section area. The surfaces of the samples were also polished and examined with an optical microscopy to assess the underlying fibre orientation of each specimen group. The examined surfaces were chosen on the transverse and longitudinal planes with respect to the specimen axis, which also corresponds to the loading direction. Several micrographs at different magnitudes were acquired, covering the entire cross section of the samples. In addition, the fracture surfaces of the specimens failed under quasi-static and fatigue loading conditions were investigated by scanning electron microscopy (SEM), employing a Cambridge S260 microscope. The quasi-static failure surface was observed for specimens belonging to the HM and LM group while the fatigue failure surface was studied for specimens belonging to the HM, IM and LM groups, chosen both for short-term (i.e., cycles-to-failure between $5 \cdot 10^2$ and $5 \cdot 10^3$) and long-term cyclic failures (i.e., cycles-to-failure between $4 \cdot 10^5$ and 10^6). The SEM micrographs were taken after gold sputtering the specimen fracture surface.

3. Results and discussion

3.1 Mechanical properties and fibre orientation

Results of the preliminary investigation on elastic modulus are summarized in Fig.1. As anticipated, the material exhibits a high variation of the elastic modulus. The range of values is approximately between 5600 and 24000 MPa. Compared to the values reported in a previous study for neat PEEK (i.e., 3825 MPa)[3] the observed

values are always higher and, even when the fibre orientation is transverse to the loading direction examined, the material is stiffer than the unreinforced polymer.

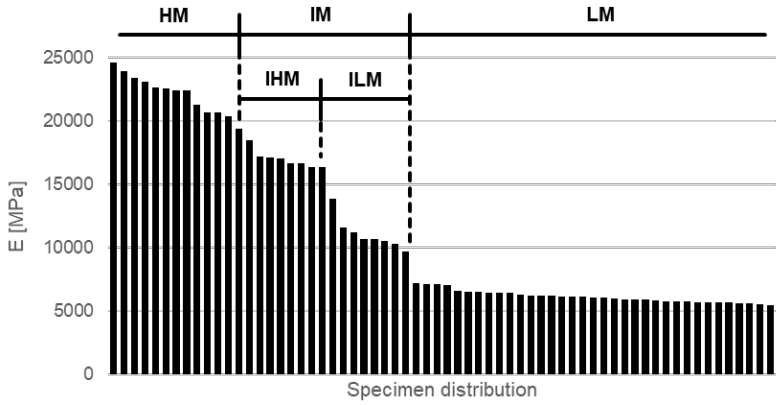

Fig.1 Distribution of Elastic Modulus E on available samples.

Polished surfaces of the samples were then analysed with an optical microscope to check the assumption that specimens with similar values of E should share similar microstructure (i.e., similar preferred fibre orientation). A representative example of the microstructure is shown in Fig.2, in which micrographs on planes that are transverse and parallel to the loading direction are combined into a perspective view. It is evident that the observed fibre distribution is very different when comparing HM, IM and LM families. In HM specimen, the fibres are almost completely aligned with the loading direction, whereas in LM samples the fibres are aligned perpendicular to the specimen axis. For IM specimens a mixed distribution is instead present. These observations support the assumption that the large variation of the elastic modulus, E, observed in the specimens depends on the different microstructural architectures.

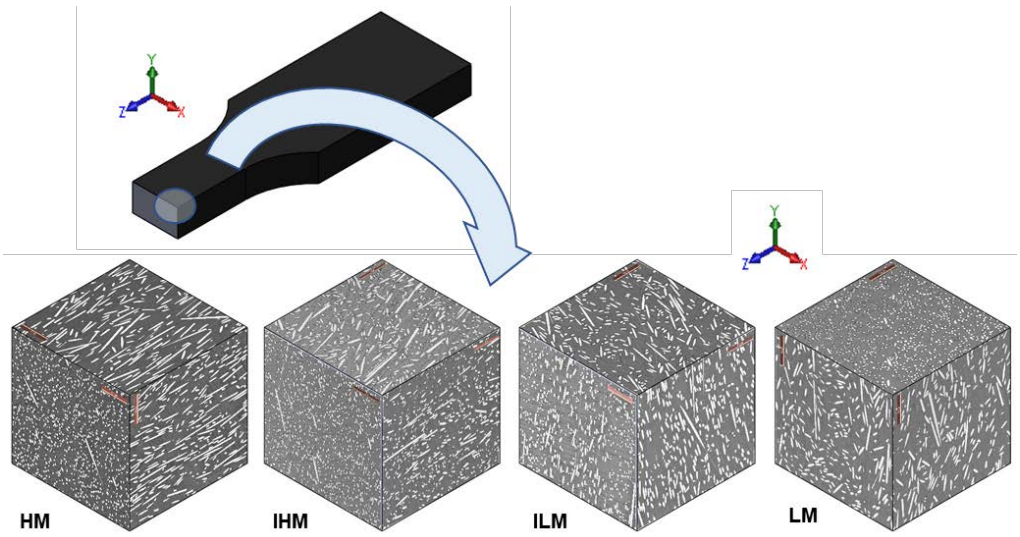

Fig.2 Representative fibre distribution on samples with different elastic modulus E (200X magnitude micrographs).

Micrographs taken on transversal sections (perpendicular to specimen axis) were also analysed with in-house developed scripts for digital image processing. By counting the number of fibres with a circular profile (i.e., aligned perpendicularly to the image plane), an estimate of the relative quantity of fibres aligned with the specimen axis could be obtained. Then, a volume fraction referred only to aligned fibres (V_{fal}) was defined as the ratio between the area of this subset of fibres and the total area of the corresponding image. For the LM sample the fibres were almost completely lying on planes perpendicular to the loading direction ($V_{fal} \approx 0.2\%$), while for HM samples the opposite condition was observed with the fibres being almost aligned with the specimen axis ($V_{fal} \approx 22\%$). These highly oriented fibre distributions are associated with the lower and upper bounds of the elastic modulus. For IM samples, a mixed distribution was observed (V_{fal} in the range 10 ÷18 %), in line with the intermediate values of E (see Fig.3).

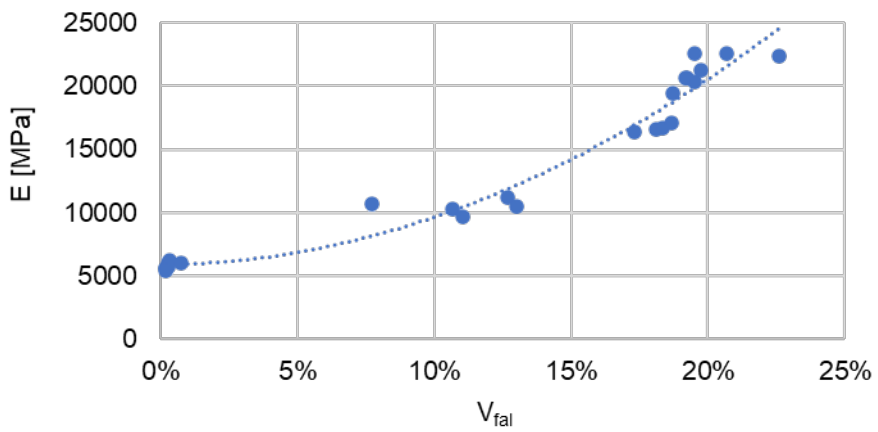

Fig.3 Elastic modulus E vs. $V_{fal.}$

These experimental results can also be compared with analytical models for the prediction of Young's modulus in SFR composites. While many modelling approaches can be found in literature, the shear lag models provide a simple way to estimate the elastic modulus (see [31] and [32] for detailed reviews). More specifically, one of the most commonly used is the Cox-Krenchel model, in which the elastic modulus is predicted by a modified rule of mixture, as per eq. (1):

$$E = \eta_l \eta_o E_f V_f + E_m (1 - V_f) \qquad (1)$$

where η_l and η_0 represent the fibre length efficiency factor and the fibre orientation efficiency factor. The coefficient η_0 ranges between the unit value for unidirectional alignment and 0.2 for a 3D random distribution [33]. Following [32], η_l can instead be expressed as per eq. (2):

$$\eta_l = 1 - \frac{Tanh(\beta L/2)}{(\beta L/2)} \qquad (2)$$

in which L is the fibre length and β is defined by eq. (3) as:

$$\beta = \sqrt{\frac{H}{\pi r_f^2 E_f}} \qquad (3)$$

where E_f is the fibre elastic modulus, r_f is the fibre radius and H is a coefficient to be calculated with eq. (4):

$$H = \frac{2\pi G_m}{\ln\sqrt{K_R/V_f}} \qquad (4)$$

In Eq. 4, G_m is the shear modulus of the matrix, whereas K_R is a constant depending on modelling assumptions for representative volume and associated fibre packing scheme. Evidently, the implementation of this analytical model requires knowledge of several properties both for the matrix and for the fibre, which are not always available for short fibre composites. In particular, model predictions are influenced by the choice of the E_f value, which should be in the range of 180 – 240 GPa [34] and by assumptions on the fibre packing scheme, with values of K_R in the range of 0,785-3,628 [32].

The set of values reported in Tab.1 were thus either derived from literature or determined from available data with classic formulas of mechanics of materials. Applying the Cox-Krenchel model (eq. 1 and following) to the parameter set of Tab.1 led to: $\eta_l \approx 0.56$, $H \approx 6400$ MPa, $\beta \approx 5.4$ mm^{-1} and thus a Young modulus of ≈28000 MPa for the case of fully unidirectionally-aligned discontinuous fibres (i.e., $\eta_0 = 1$). This value compares favourably with the maximum value of more than 24000 MPa measured experimentally, especially when considering that the maximum $V_{fal} = 0.22$ measured on the micrographs was lower than the value of 0.237 determined theoretically. On the other hand, by setting the value of η_0 to 0.2, the predicted Young modulus for a random distribution is ≈ 8000 MPa, which is an intermediate value between the ILM and LM moduli. Again, the result compares quite favourably, especially when considering that the LM family represents a more unfavourable condition than random distribution.

Tab.1 Parameters used for the Young modulus prediction via Cox-Krenchel model.

Parameters used for the Cox-Krenchel model		
Name	**Value**	**Source**
Fibre weight fraction, W_f	0.3	Datum
Matrix density, ρ_m	1.3 g/cm^3	Ref. [35]
Fibre density, ρ_f	1.79 g/cm^3	Ref. [34]
Fibre Volume fraction, V_f	0.237	Calculated, Ref. [33]
Fibre Young Modulus, E_f	191000 MPa	Ref. [36]
Matrix Young Modulus, E_m	3825 MPa	Ref. [7]
Matrix Poisson's ratio, ν_m	0.38	Ref. [35]
Matrix Shear Modulus, G_m	1389 MPa	Calculated, Ref. [33]
Average fibre length, L	150 mm	Measured
Average fibre radius, r_f	3.5 mm	Measured
Fibre packing constant, K_R	3.628	Ref. [32]

Results of the tensile tests are summarized in Fig.4, in which the engineering stress-strain curves are reported. As already mentioned, even though the samples were taken on the same extruded plates, substantial differences can be noticed depending on the orientation and position, but no obvious correlation with plate geometry and extrusion direction could be made. In particular, the following remarks apply:

a) The six specimens selected for tensile testing exhibited considerable differences in terms of tensile strength, with an average value of 127 MPa and a standard deviation of 33 MPa. Remarkably, due to the high dispersion of results, tensile strength values for particularly unfavourable fibre orientations get closer to 97 MPa value observed for neat PEEK in our previous study [7].

b) In parallel to stiffness and strength modification, the material exhibits a pronounced shift from a ductile to a more brittle behaviour associated with an increasing alignment of the fibre with the loading direction. For LM samples, the material exhibits yielding with a marked transition from the initial elastic regime to a plastic region where a plateau stress level is reached, with failure strain up to 11%. This behaviour resembles neat PEEK, in which elongation at break can reach 15%. For samples with fibres oriented parallel to the loading axis, yielding cannot be observed clearly and elongation at break decreases to 1.6-2.5 %.

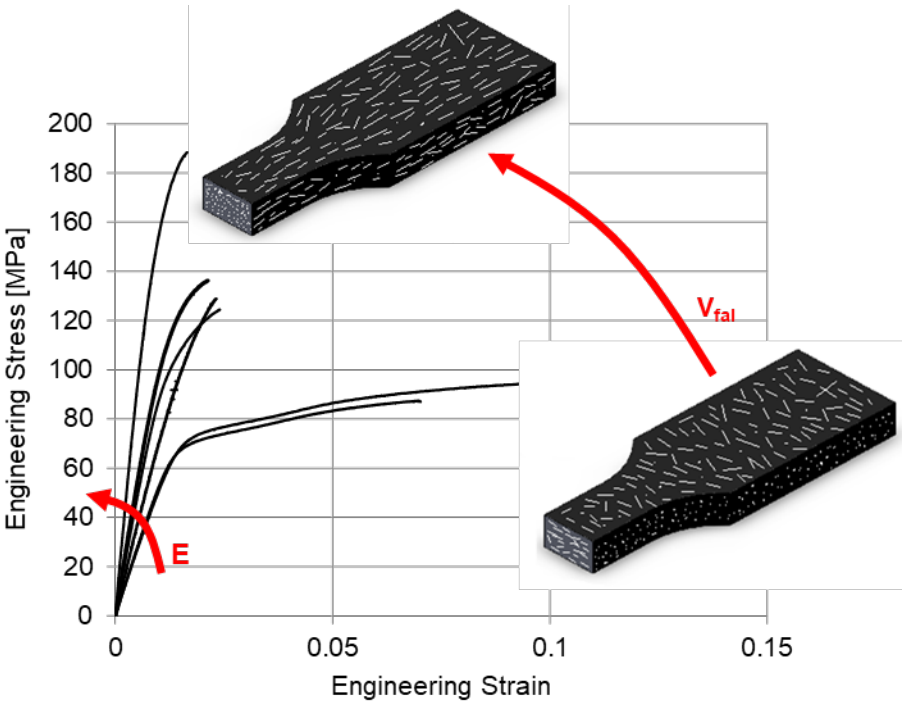

Fig.4 Stress-strain curves showing different V_{fal} influence on elastic modulus and static strength.

According to literature, anisotropy induced by preferred fibre orientation generally results in higher strength and elastic modulus in the moulding flow direction [37][17]. Results of the present investigation are in line with these findings, with a nearly sixfold increase of elastic modulus when comparing neat PEEK and specimen with almost complete fibre alignment along the loading direction. In fact, an increasing orientation of the fibres with the specimen axis clearly correlated with higher elastic modulus, up to a max/min ratio of ≈ 6, and higher tensile strength, up to a value of 190 MPa corresponding to a max/min ratio > 2. Overall, these observations support the assumption that the degree of fibre orientation is a driving factor influencing the mechanical behaviour of SFR polymer composites, of course in combination with other factors such as fibre content and length and effects of viscous properties of the matrix on processing flow conditions.

3.2 Fatigue testing

3.2.1 Cyclic stress-strain response and damage evolution

When subjected to cyclic loading, SFR thermoplastics may exhibit substantial modification of their mechanical response, because of evident damage accumulation.

A comparative example of cyclic stress-strain loops for LM and HM groups is shown in Fig.5 for different stress levels. The observed cyclic response is characterized by hysteresis loops that are typical of composite materials with viscoelastic matrix and the shape, size, and position of stress-strain loops change during cyclic loading. Unfortunately, a direct comparison for the same stress level is not possible, because stress ranges for the different families were only partially overlapping. However, these effects are noticeable for LM family, even if the applied stress is significantly lower. As could be expected for a load-controlled tension–tension cyclic test, stress-strain loops also moved along the strain axis throughout most of the life of the specimen, resulting in cyclic creep (i.e. mean value of strain, ε_m, may progressively shift along the strain axis). The presence of cyclic creep for the examined material was already reported in in our previous study [7] and was also noticed in the present work. In this respect, the sensitivity on the preferred fibre orientation clearly emerged again: the lower the elastic modulus, the larger the shift of the stress-strain cycle during the tests, despite the more compliant families being tested at lower stress levels.

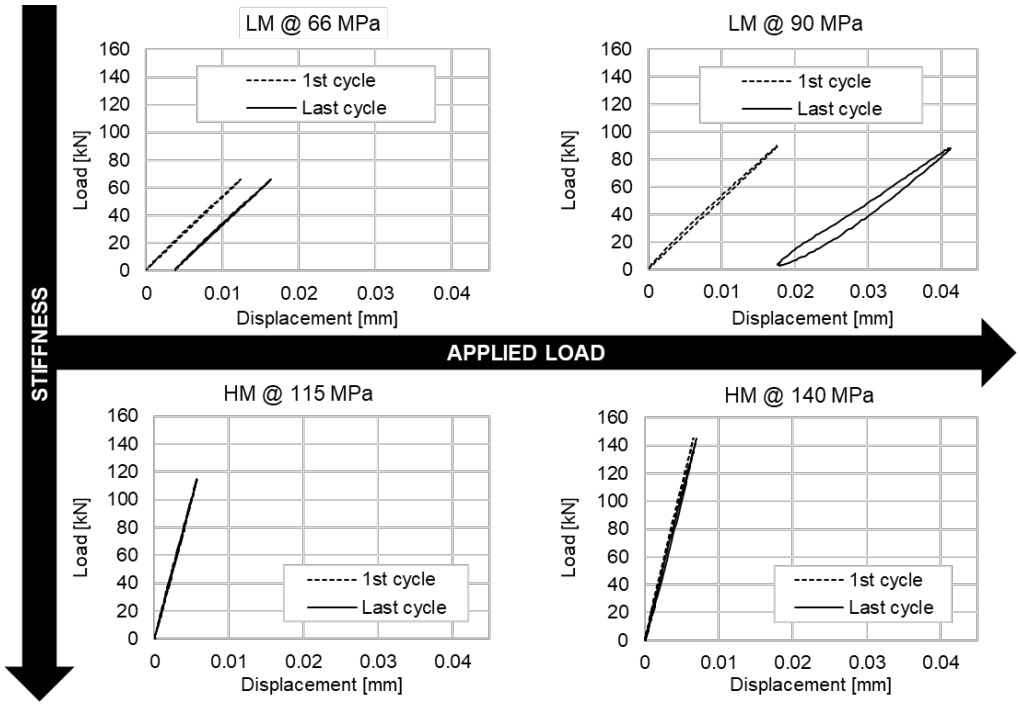

Fig.5 Cyclic stress strain loops for four representative scenarios: lowest and highest stress levels for both lowest and highest modulus families (LM and HM)

Due to the viscoelastic nature of the matrix, a possible reason of shape and size changes of the load-displacement cycle curve could be an increase of temperature caused by hysteretic heating, which may also lead to stiffness degradation, due to the temperature dependency of the elastic modulus typical of thermoplastic polymers. As

already observed in a previous investigation [7], the temperature raise over ambient for the material under investigation is actually limited to 5÷15 °C and the material tends to reach thermal equilibrium. While specimen temperature may affect the fatigue failure mechanism when the combination of load, frequency and material thermal properties results in excessive heating [38], it should be noted that this type of failure was never observed in the present study. Having determined that the temperature-related decrease of stiffness is limited, the fatigue behaviour of SFR-PEEK was examined by analysing stiffness reduction associate to the evolution of the stress–strain cycle during the tests. In load-controlled tests, because of material damage, the amplitude of the strain range Δε due to the imposed and constant stress range Δσ may increase with increasing cycle number. At a macroscopical level, this results in a reduction of specimen stiffness and the progressive modification of the stress–strain loop amplitude can be simply described by a damage index D as per eq. 5 [39]:

$$D(N) = 1 - \frac{E^*(N)}{E_0^*} \qquad (5)$$

where $E^*(N)$ is the apparent elastic modulus of a cycle and E_0^* is its initial value. The apparent elastic modulus represents the average slope of a full cycle and corresponds to its linear regression. The evolution of the damage index is shown in Fig.6, evidencing a non-constant slope of the D–N curve, and one can recognize the presence of regions with different damage rates. According to [40], for short glass fibre reinforced thermoplastics, fatigue damage evolution occurs under three stages. At first, a high stiffness reduction occurs during the initial cycles due to the formation of matrix micro-voids. During the second stage, the coalescence of microcracks takes place which gives a gradual stiffness reduction of the material. During the last stage, fibre fracture and macroscopic crack propagation occurs, resulting in a rapid stiffness reduction and leading to final fracture. Considering the SFR-PEEK under investigation, the different families could be compared only on partially overlapping stress ranges, because of their remarkably different fatigue strengths. Nevertheless, some interesting observations can be made on the influence of fibre orientation on progressive failure mechanisms. The above-mentioned damage-evolution model seems to fit, at least partially, the response of LM and ILM families. In fact, after the initial transitory, a prolonged stage is present in which a lower and more constant slope can be observed and then, in a final stage, the slope of D–N curve tends to increase as final failure approaches. For higher stress level the pattern of damage evolution is still similar but with a significant increase of damage rate and consequent reduction of the duration of the intermediate stage.

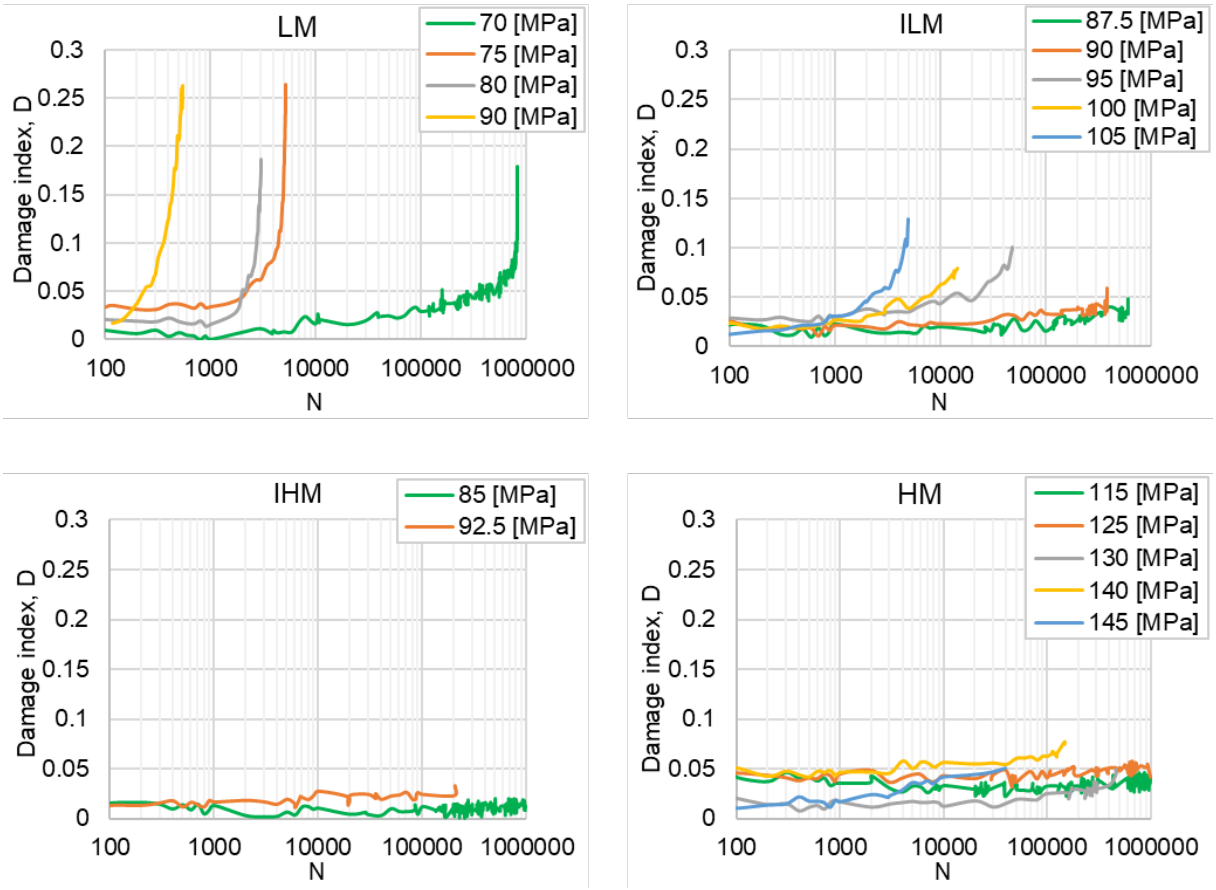

Fig.6 Damage evolution for different SFR-PEEK classes

In particular, for LM specimens, the fibres are oriented mostly transverse to the loading direction and the damage curve is smoother. This could possibly correspond to a faster rate of formation and progressive coalescence of defects in the matrix because of the reduced contrasting effect of the fibres or even of their negative action as stress-concentration points. In ILM samples, the number of fibres oriented in the loading direction slightly increases, and the positive counteracting effect of the fibre is little bit more pronounced. As a result, the damage rate is lower, except for the last stage in which final failure is approached. When considering IHM and HM families a substantially different behaviour is observed. Despite the material being tested at higher stress levels, only a limited (if any) increase of the damage index could be observed, with lower damage rates and no significant change along the test. Here, the positive influence of the fibres is more noticeable. In this case, even if the stress levels are higher, no significant effect can be appreciated on the stiffness suggesting that damage to the matrix is limited by the counteracting action of the fibres, which on the one hand limit matrix deformation and microcracks nucleation and on the other prevent or retard crack coalescence by acting as obstacles to the crack

growth. Similarly, and still in contrast with LM and ILM, the HM and IHM families are showing little to no cyclic creep (see Fig.5).

3.2.2 Fatigue life curves

The results of fatigue tests for the different families are summarized in Fig.7, in the form of S_{max}-N_f curves with log-log coordinates, with S_{max} being the peak stress of the loading cycle. Experimental data were processed referring to methods described in the Standard ISO 12107. The upper and lower bounds of the S_{max}-N_f curve in the finite life regime, as reported in Fig.7, were calculated with a 95% confidence. Overall, despite having a small number of specimens, especially for IHM family, the S_{max}-N_f curve resulting from experimental data showed low dispersion.

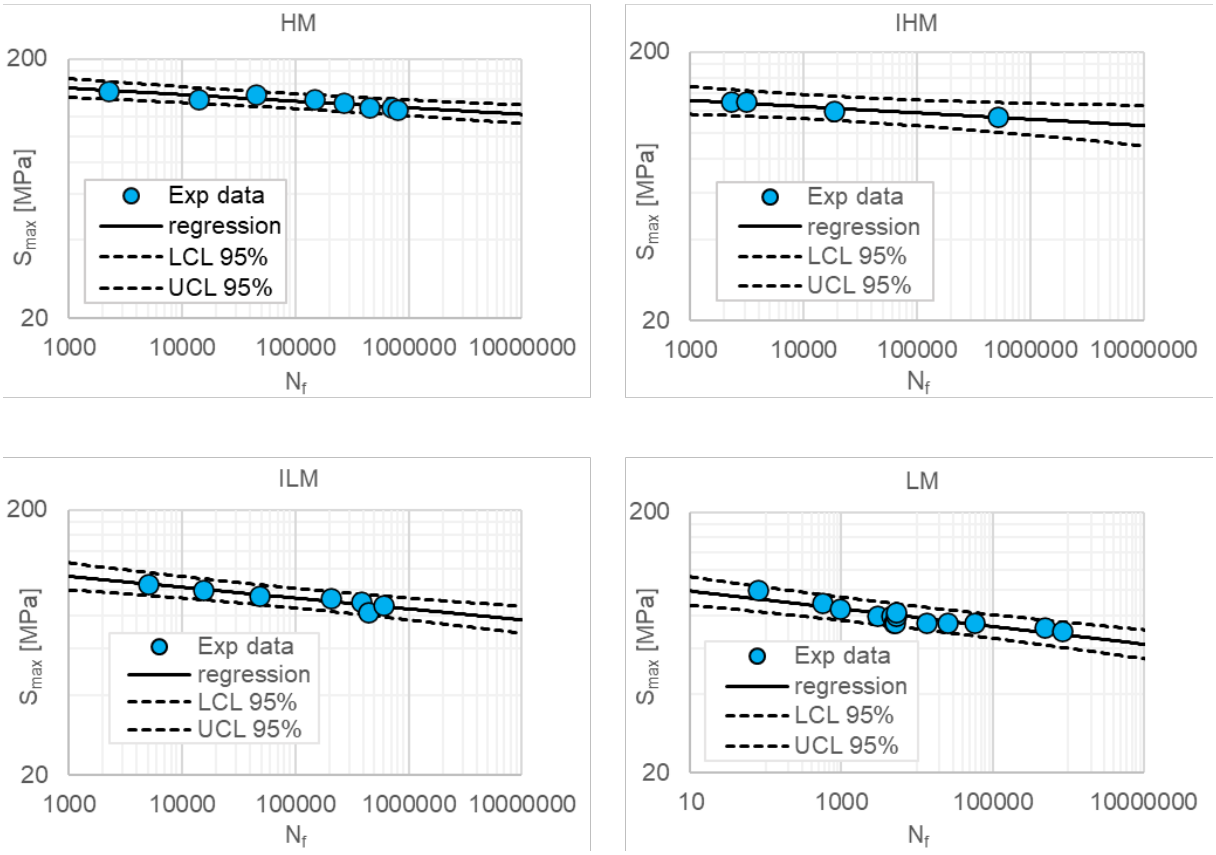

Fig.7 Fatigue life curves for each specimen family. The regression line represents the fit as per eq.6 and LCL and UCL represent the lower and upper confidence limits respectively.

The differences between the four families HM, IHM, ILM and LM are clear. The elastic modulus grouping allowed the observation of a distinct trend with limited dispersion for each family. Overall, even if for some

families the number of sample available is limited, the results of the fatigue tests show the presence of a strong correlation between fatigue strength and elastic modulus and, consequently, between fatigue strength and fibre spatial arrangement. The sample size is particularly small for the IHM family where only 4 samples were tested. However, one should remember that the sample size of each family could not be predicted a-priori, therefore the samples resulted randomly distributed over the four families. Fatigue data were then fitted with the typical Basquin-like equation (eq. 6) [41] which is also proposed by the abovementioned Standard ISO 12107:

$$S_{max} = A\left(N_f\right)^B \qquad (6)$$

where S_{max} is the peak stress, N_f is the number of cycles to failure, and A and B are material constants. Taking base-ten logarithms provides (eq. 7):

$$\mathrm{Log}(S_{max}) = \mathrm{Log}(A) + B\,\mathrm{Log}(N_f) \qquad (7)$$

which allows for a linear regression of the experimental results in finite life regime and clearly shows that B and Log(A) represent respectively the slope and the intercept of the linear regression. Results are summarized in Tab.2, including neat PEEK from our previous study [7] for comparison purposes, in which E is the average modulus and the estimated fatigue limit at 10^6 cycles is also reported.

Tab.2 Fitting parameters of fatigue curve.

	E [MPa]	B ± std.dev.	A ± std.dev.	Estimated fatigue limit at 10^6 cycles [MPa]
HM	21490	-0.025 ± 0.0046	183 ± 4.4	130
IHM	16610	-0.023 ± 0.0050	155 ± 4.1	110
ILM	10960	-0.041 ± 0.0070	149 ± 5.0	85
LM	5730	-0.034 ± 0.0050	108 ± 2.7	70
NEAT	3800	-0.03 ± 0.011	122 ± 6.6	75

In Fig.8(a) a comparison between LM, IM and HM modulus families is provided. From Fig.8(a) and Tab.2, it is clear that an extremely high dispersion of the data would have been observed without the preliminary stiffness classification. In Fig.8(b), the fatigue data for SFR-PEEK are reported considering the Strain Energy Density (SED) associated with each stress and the initial strain level of the test, defined as per eq. 8:

$$SED = \frac{1}{2}\sigma\varepsilon_0 = \frac{1}{2}\frac{\sigma^2}{E_0} \qquad (8)$$

in which the material is assumed to remain in the linear elastic regime, E_0 is the initial elastic modulus of the specimen (referred to loading direction) and ε_0 is the initial nominal strain value associated with imposed nominal stress σ.

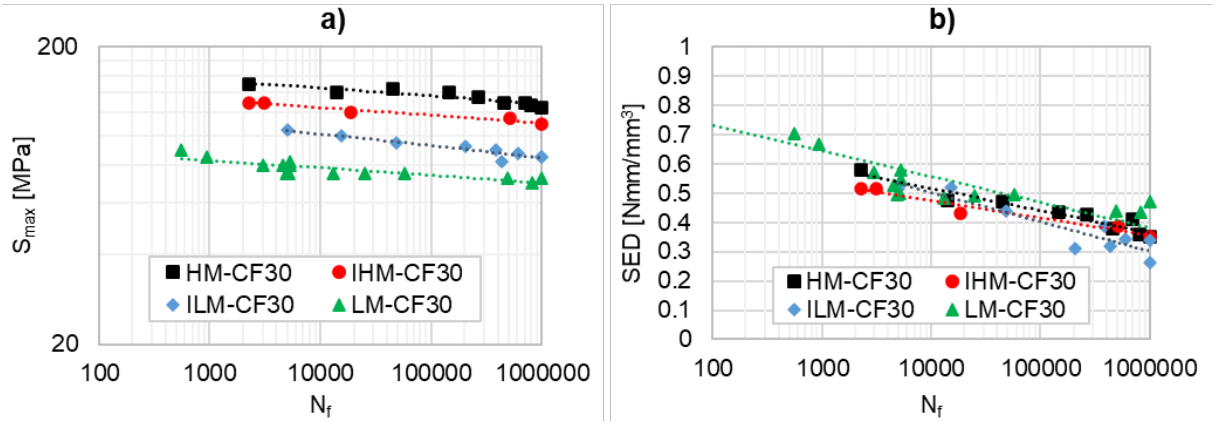

Fig.8 (a) S_{max}-N curve, (b) SED-N

Quite interestingly, in this case, despite substantial changes in the elastic modulus and strength values, the differences between the various families of CF30 are much less evident. The reason of this behaviour can be understood by considering that the SED includes the effects of the elastic modulus. From a design point of view this may suggest that SED could function as a reference quantity to develop unified fatigue failure criteria applicable to otherwise distinct materials. Considering our data in comparison with literature, higher fatigue strength is usually associated with the preferred orientation of the fibre aligned with applied load direction [21]. As an example, when comparing specimens with a preferred fibre orientation transverse to the loading direction with specimens having fibre mostly aligned with specimen axis, a fatigue strength reduction up to 50% were reported in [22, 42, 43]. Results of the present study are in line with these findings since the fatigue strength of the LM family is reduced by 45% when compared with the HM family. Some authors found that fatigue strengths were proportional to the corresponding tensile strength values [22], whereas in [44] the anisotropic material response was found to be less pronounced under cyclic loading rather than quasi-static loading. In the present work, the anisotropic response is marked both in static and fatigue tests and fatigue strength seems strongly correlated with the elastic modulus, as indirectly reflected by the lower dispersion observed when data are presented as SED-N curves. The slope of S-N curves in the finite life region has been reported to be steeper in the transverse samples, as compared to the longitudinal samples [45], whereas others reported that S-N curves

were nearly parallel for different orientation angles [22]. In the present study LM and ILM families showed a steeper slope, whereas IHM and HM were nearly parallel. It should be noted that most of the published literature on this aspect concerns short glass fibre reinforced polyamides, in which the effects of fibre orientation were examined by cutting the samples at different angles or positions of injection moulded plates. However, to the best of the authors' knowledge, there is a lack of data concerning fatigue strength for PEEK and more specifically correlations with fibre orientation. Published investigations are limited to rotating–bending fatigue tests on plain and notched specimens of neat and short carbon–fibre reinforced PEEK described in [12]. More recently, authors considered fatigue, damage and notch effects for extruded PEEK composites in previous works [7], but influence of the fibre orientation was not investigated. The present research provides therefore new insights on the fatigue of SFR PEEK. In particular, since the different behaviours are clearly associated with fibre orientation, our results could be interpreted as the consequence of contrasting effects of the fibre reinforcement phase, in particular as a function of their orientation with respect to loading direction. On the one hand, short fibres may have a positive effect, by increasing strength of the material, increasing stiffness, and thus reducing matrix strain for a given level of applied stress and acting as obstacles to crack propagation. On the other hand, fibres may also exert a negative effect by acting as stress raisers and inherent small internal defects. The positive effect is clearly prevalent when fibres are oriented parallel to the loading direction: the material is stiffer and the matrix undergoes lower strain levels thus decreasing the risk of crack nucleation in the matrix. During the crack propagation phase, their action as obstacles to crack propagation is fully exploited, since, the rate of crack propagation perpendicular to aligned fibres is much slower than that parallel to the fibres when compared at the same stress intensity range, as documented in [23]. The negative effect is instead prevailing when the fibres are predominantly oriented transversely to the loading direction. In this case, and for the same stress level, the matrix undergoes higher deformation, and the propagation of the fatigue crack is not counteracted by the fibres, which may act instead as discontinuities. This could explain the detrimental effect observed when comparing LM CF30 fatigue strength with neat PEEK. Of course, as shown in [20] and [28, 29], for this class of material, fatigue crack resistance has a complex interdependence of various matrix-related factors, such as molecular weight, crystallinity and fibre type: length, aspect ratio, and preferred orientation. For a thorough review on the many factors influencing cyclic deformation, fatigue behaviour, and damage development of SFR polymer composites the interested reader can refer to [28], in which both microstructural and loading related effects were considered.

Finally, it should be noted that findings of the present work refer to a fixed value of fibre weight fraction W_f. Although it could be reasonably inferred that the presence of a preferred fibre alignment should result in anisotropic fatigue strength even for different values of W_f, in practice the extension of the research to different W_f would necessarily require further testing. In fact, both the possible relationship between the amount of fibre aligned along a preferred direction and the nominal value of W_f, both the balance between contrasting actions of the fibres as a function of W_f, should be investigated.

3.2.3 Fracture surfaces and failure mechanism

The electron scanning microscope was employed to study the fracture surfaces developed for the various specimen types (HM; IM; LM) under specific failure conditions (tensile quasi-static failure; long-term cyclic failure; short-term cyclic failure). Fracture surfaces developed under tensile quasi-static loading are represented in Fig.9 for HM and LM specimens, at three magnification levels.

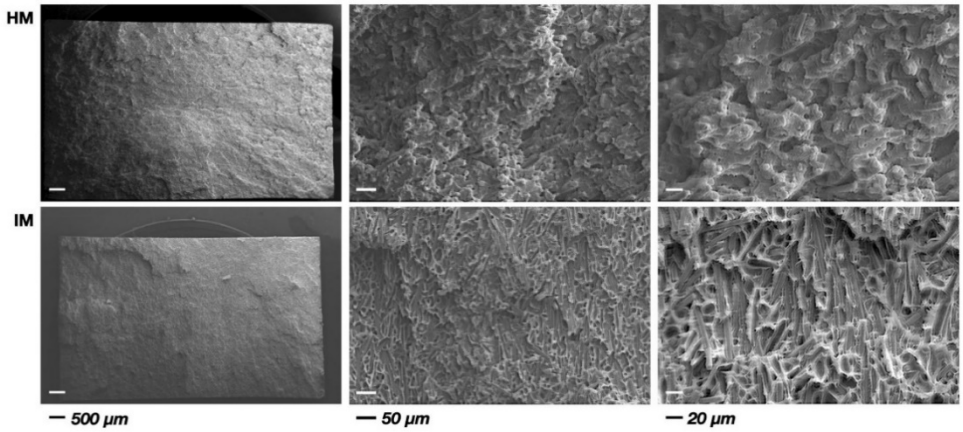

Fig.9 SEM micrographs at various magnifications of the fracture surfaces in the case of quasi-static tensile failure of HM and LM specimen.

Observation at the macro-scale suggest a clear difference for the two specimens, and, in particular, a wider and diffuse roughness in the case of the HM specimen, and a flatter and more regular surface in the case of the LM one. Higher magnifications also revealed different micro-structures and, thus, different failure mechanisms for the two specimens. The fracture surface of the HM specimen displays a large fraction of protruding fibres, oriented perpendicularly to the fracture surface, or slightly angled with respect to the normal direction. The emerging fibres seem to be well bonded with the matrix, and failure seems to be more likely associated to void formation in the matrix than to the fibre pull-out, suggesting that cracking is due to initiation of micro-cracks in

the matrix and to fracture of the fibres, similarly to what observed in [46]. By contrast, the LM specimen reveals a fibre orientation almost completely perpendicular to the loading direction. The presence of both debonded fibres and fibre-like voids on the fracture plane suggests that the failure mode in this case mainly regards the fibre-matrix interface. Evident signs of plasticity close to the fibre-matrix interface and microvoids highlight the occurrence of local plasticity before debonding. This type of mechanism is responsible of the flatter fracture surface for the LM specimen and mainly involves planar failure events. A partially different scenario is revealed in the case of fatigue loading: Fig.10 displays, for the three families, the fracture surface for long-term fatigue failure (i.e., cycles-to-failure between $4 \cdot 10^5$ and 10^6), associated with low applied load amplitudes.

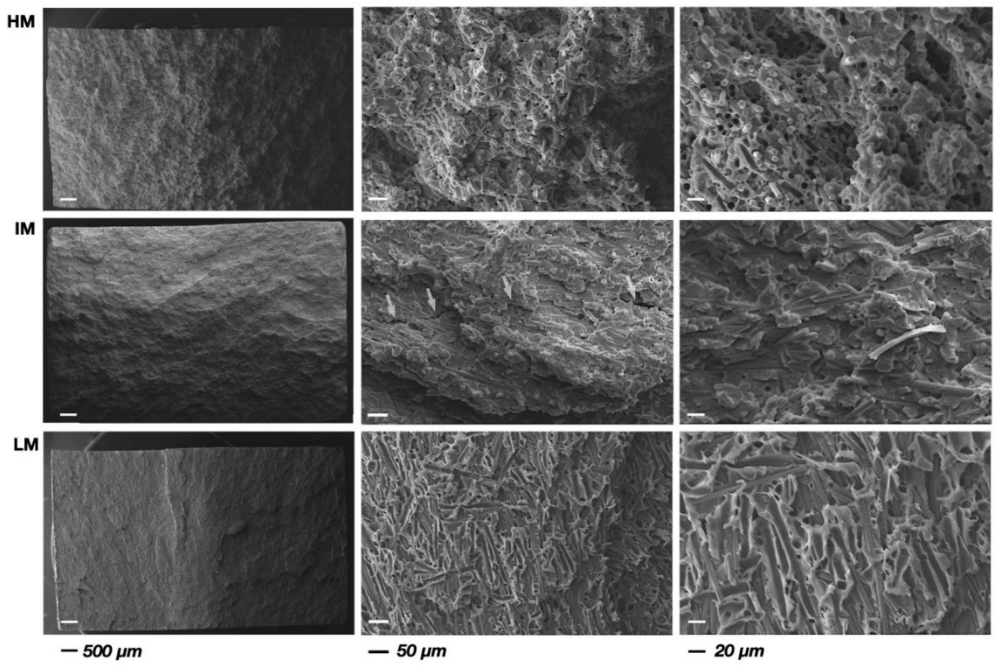

Fig.10 SEM micrographs at various magnifications of the fracture surfaces in the case of long-term cyclic failure of the three types of material batches: HM (cycles-to-failure: 801428; $\Delta\sigma$ = 127.5 MPa); IM (cycles-to-failure: 436253; $\Delta\sigma$ = 82.5 MPa); LM (cycles-to-failure: 823237; $\Delta\sigma$ = 70 MPa).

The low load amplitude condition, being less critical for the material, allows a suitable time scale for the fatigue damage mechanism to be developed and to reveal the peculiar differences between quasi-static and fatigue failure conditions. In all the cases no sign of a critical initial, or predominant, crack is shown, nor of a propagation region, suggesting that the failure takes place on a local scale through a cumulative damage. In the case of the HM specimen, the fracture surface shows a moderate roughness at the macro-scale. Higher magnifications evidence a microstructure consisting of fibres mainly oriented perpendicularly to the fracture

surface. The large number of voids, with size consistent with the fibre diameter, suggests the occurrence of fibre debonding and pull-out as most relevant failure mechanisms, accompanied by occasional debonding of transversely oriented fibres, when present. By contrast, the LM fracture surface shows, globally, less roughness and a more planar fracture region. On the micro-scale this corresponds to the occurrence of fibre-matrix debonding and matrix plasticity, similar to the quasi-static loading. The fracture of the surface of the IM specimen seems to present all the aforementioned failure mechanisms. At the macro-scale, the surface shows a moderate roughness, while on the micro-scale all the mechanisms seem to take place: pull-out of the more loading-aligned fibres; debonding of the transversely oriented fibres; cavitational micro-cracks in the matrix; cracking of the fibres. However, in this case, the failure seems to occur at a larger scale than that of the fibre-matrix interface, involving large agglomerates of fibres and matrix. This is suggested by the development of cracks between these agglomerates (see arrows in the intermediate picture of the IM series), propagating through the matrix and bridged by fibres.

Fig.11 shows the fracture surface developed at a low cycle number (i.e., cycles-to-failure between 5102 and 5103), obtained on specimens subjected to the highest load amplitudes. The fracture surface, in this case, present overall a less regular appearance with respect to those created by longer fatigue life. The surface irregular aspect becomes less pronounced when moving from HM to IM, and finally to LM specimens. The HM surface displays again a large number of fibres emerging from the fracture plane, confirming fibre debonding and pullout as failure mechanisms. However, with respect to the long-term fatigue, a larger number of transverse fibres and fibre-like voids lying on the surface plane are present, revealing that also mechanisms of transverse failure become important to the final rupture and suggesting that the peculiar surface roughness may be due to a multi-layered fracture process based on transverse failure. The IM specimen fracture surface confirms the occurrence of a process that mainly involves agglomerates of randomly oriented fibres bundled by the matrix. Fibres on the outer surface are mainly lying on the fracture plane and indicates transverse failure as the most relevant failure mechanisms at the agglomerates' interfaces. Finally, the LM surface mainly displays fibre lying transversally to the applied load, with sign of matrix-fibre debonding and cavitation in the matrix. However, with respect to the long-term fatigue, the fracture mechanisms show a more brittle failure, with no evident signs of plasticity in the matrix. Furthermore, fracture seems to be less planar and originating on more planes simultaneously, leading to the increased surface roughness.

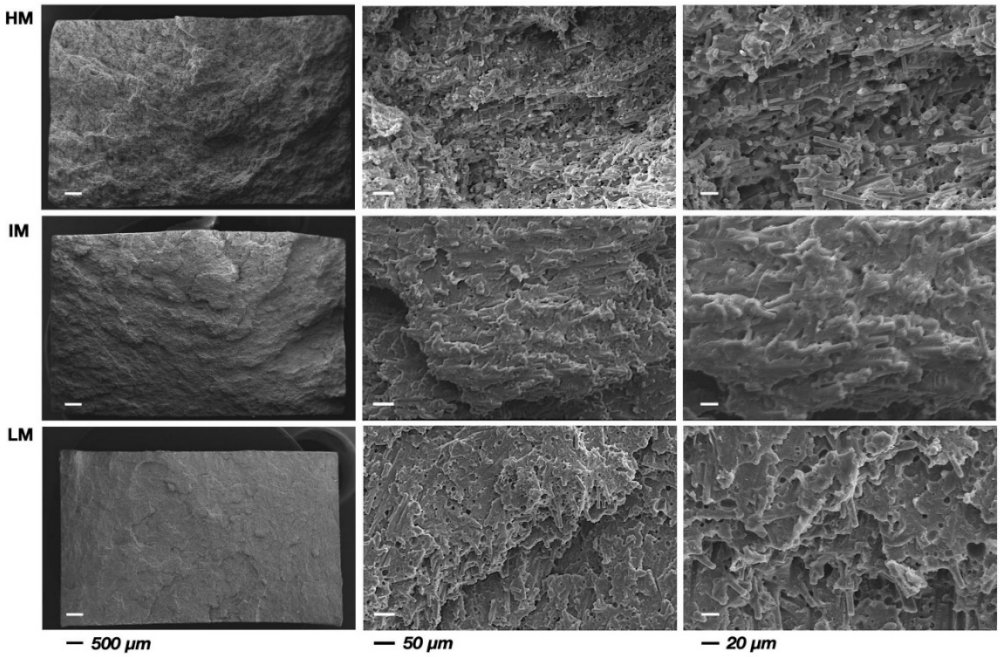

Fig.11 SEM micrographs at various magnifications of the fracture surfaces in the case of short-term cyclic failure of the three types of material batches: HM (cycles-to-failure: 2261; $\Delta\sigma$ = 150 MPa); IM (cycles-to-failure: 4994; $\Delta\sigma$ = 105 MPa); LM (cycles-to-failure: 552; $\Delta\sigma$ = 90 MPa).

4. Conclusions

As a consequence of processing, extruded short carbon fibre reinforced PEEK may exhibit a highly heterogeneous microstructure, with presence of different degree of fibre alignment with respect to specimen axis. This heterogeneity leads to different static and fatigue properties depending on whether the preferred orientation of the fibre is parallel or perpendicular to the loading direction. In particular, the elastic modulus can range from 5600 to 24000 MPa while the tensile strength can range from 97 to 180 MPa, with higher stiffness and strength observed when higher quantities of fibre are oriented along the loading axis. Similarly, preferred fibre orientation dictates fatigue behaviour with the estimated fatigue limit ranging from 70 to 130 MPa for fatigue tests with R=0. The underlying evolution of damage and failure mechanisms are also clearly associated with fibre orientation and suggest that the observed behaviour could be the consequence of contrasting effects. The reinforcing effect of short fibres is prevalent when fibres are oriented parallel to the loading direction, resulting in increased strength and stiffness and in a reduction of matrix strain for a given level of applied stress. Moreover, fibres can also positively act as obstacles to crack propagation. However, fibres that are oriented perpendicularly to loading can exert a negative effect on fatigue resistance, resulting in lower fatigue

performances than neat material, by acting as stress raisers and inherent small internal defects, with limited capability to counteract crack propagation. Overall, from a design point of view, these results highlight that improvements in fibre direction control, by tuning of process parameters, may potentially lead to a high-performance material. Therefore, assessing fibre distribution is of paramount importance to completely exploit the potential of the material, both to associate a correct value of stiffness and allowable strength to the chosen material, avoiding over-conservative assumptions or overconfident safety factor predictions, and to select proper constitutive modelling approaches.

References

1. Sarasua, J.R., Remiro, P.M., Pouyet, J.: The mechanical behaviour of PEEK short fibre composites. J. Mater. Sci. 30, 3501–3508 (1995). https://doi.org/10.1007/BF00349901

2. Li, F., Hu, Y., Hou, X., Hu, X., Jiang, D.: Thermal, mechanical, and tribological properties of short carbon fibers/PEEK composites. High Perform. Polym. 30, 657–666 (2018). https://doi.org/10.1177/0954008317715313

3. Avanzini, A., Donzella, G., Mazzù, A., Petrogalli, C.: Wear and rolling contact fatigue of PEEK and PEEK composites. Tribol. Int. 57, 22–30 (2013)

4. Kurtz, S.M., Devine, J.N.: PEEK biomaterials in trauma, orthopedic, and spinal implants. Biomaterials. 28, 4845–4869 (2007). https://doi.org/10.1016/j.biomaterials.2007.07.013

5. Aggogeri, F., Avanzini, A., Borboni, A., Pandini, S.: A robot gripper in polymeric material for solid micro-meso parts. Int. J. Autom. Technol. 11, (2017). https://doi.org/10.20965/ijat.2017.p0311

6. Liang, Q.Q., Wu, X.Q.: Research Status of Carbon Fibre-Reinforced PEEK Composites. Adv. Mater. Res. 834–836, 225–228 (2013). https://doi.org/10.4028/www.scientific.net/AMR.834-836.225

7. Avanzini, A., Donzella, G., Gallina, D., Pandini, S., Petrogalli, C.: Fatigue behavior and cyclic damage of peek short fiber reinforced composites. Compos. Part B Eng. 45, 397–406 (2013). https://doi.org/10.1016/j.compositesb.2012.06.008

8. Shrestha, R., Simsiriwong, J., Shamsaei, N., Moser, R.D.: Cyclic deformation and fatigue behavior of

polyether ether ketone (PEEK). Int. J. Fatigue. 82, 411–427 (2016). https://doi.org/10.1016/j.ijfatigue.2015.08.022

9. Noguchi, H., Kim, Y.-H., Nisitani, H.: On the cumulative fatigue damage in short carbon fiber reinforced poly-ether-ether-ketone. Eng. Fract. Mech. 51, 457–468 (1995). https://doi.org/10.1016/0013-7944(94)00282-M

10. Bonnheim, N., Ansari, F., Regis, M., Bracco, P., Pruitt, L.: Effect of carbon fiber type on monotonic and fatigue properties of orthopedic grade PEEK. J. Mech. Behav. Biomed. Mater. 90, 484–492 (2019). https://doi.org/10.1016/j.jmbbm.2018.10.033

11. Avanzini, A., Petrogalli, C., Battini, D., Donzella, G.: Influence of micro-notches on the fatigue strength and crack propagation of unfilled and short carbon fiber reinforced PEEK. Mater. Des. 139, 447–456 (2018). https://doi.org/10.1016/j.matdes.2017.11.039

12. Nisitani, H., Noguchi, H., Kim, Y.-H.: Evaluation of fatigue strength of plain and notched specimens of short carbon-fiber reinforced polyetheretherketone in comparison with polyetheretherketone. Eng. Fract. Mech. 43, 685–705 (1992). https://doi.org/10.1016/0013-7944(92)90001-U

13. Sobieraj, M.C., Murphy, J.E., Brinkman, J.G., Kurtz, S.M., Rimnac, C.M.: Notched fatigue behavior of PEEK. Biomaterials. 31, 9156–9162 (2010). https://doi.org/10.1016/j.biomaterials.2010.08.032

14. Fu, S.Y., Lauke, B., Mäder, E., Yue, C.Y., Hu, X.: Tensile properties of short-glass-fiber- and short-carbon-fiber-reinforced polypropylene composites. Compos. Part A Appl. Sci. Manuf. 31, 1117–1125 (2000). https://doi.org/10.1016/S1359-835X(00)00068-3

15. Mlekusch, B., Lehner, E.A., Geymayer, W.: Fibre orientation in short-fibre-reinforced thermoplastics I. Contrast enhancement for image analysis. Compos. Sci. Technol. 59, 543–545 (1999). https://doi.org/10.1016/s0266-3538(98)00102-x

16. Hamanaka, S., Yamashita, K., Nonomura, C., Thi, T.B.N., Wakano, T., Yokoyama, A.: Measurement of fiber orientation distribution in injection-molded composites with high filler content. AIP Conf. Proc. 1914, 1–6 (2017). https://doi.org/10.1063/1.5016776

17. Rolland, H., Saintier, N., Wilson, P., Merzeau, J., Robert, G.: In situ X-ray tomography investigation on damage mechanisms in short glass fibre reinforced thermoplastics: Effects of fibre orientation and

relative humidity. Compos. Part B Eng. 109, 170–186 (2017). https://doi.org/10.1016/j.compositesb.2016.10.043

18. Bernasconi, A., Cosmi, F., Hine, P.J.: Analysis of fibre orientation distribution in short fibre reinforced polymers: A comparison between optical and tomographic methods. Compos. Sci. Technol. 72, 2002–2008 (2012). https://doi.org/10.1016/j.compscitech.2012.08.018

19. Rinaldi, M., Ghidini, T., Cecchini, F., Brandao, A., Nanni, F.: Additive layer manufacturing of poly (ether ether ketone) via FDM. Compos. Part B Eng. 145, 162–172 (2018). https://doi.org/10.1016/J.COMPOSITESB.2018.03.029

20. Karger-Kocsis, J., Friedrich, K.: MICROSTRUCTURE AND FRACTURE TOUGHNESS OF SHORT FIBRE REINFORCED INJECTION-MOULDED PEEK COMPOSITES. Plast. Rubber Process. Appl. 8, 91–104 (1987)

21. Mortazavian, S., Fatemi, A.: Fatigue behavior and modeling of short fiber reinforced polymer composites including anisotropy and temperature effects. Int. J. Fatigue. 77, 12–27 (2015). https://doi.org/10.1016/j.ijfatigue.2015.02.020

22. Bernasconi, A., Davoli, P., Basile, A., Filippi, A.: Effect of fibre orientation on the fatigue behaviour of a short glass fibre reinforced polyamide-6. Int. J. Fatigue. 29, 199–208 (2007). https://doi.org/10.1016/j.ijfatigue.2006.04.001

23. Tanaka, K., Kitano, T., Egami, N.: Effect of fiber orientation on fatigue crack propagation in short-fiber reinforced plastics. Eng. Fract. Mech. 123, 44–58 (2014). https://doi.org/10.1016/J.ENGFRACMECH.2014.03.019

24. Dean, A., Reinoso, J., Sahraee, S., Rolfes, R.: An invariant-based anisotropic material model for short fiber-reinforced thermoplastics: Coupled thermo-plastic formulation. Compos. Part A Appl. Sci. Manuf. 90, 186–199 (2016). https://doi.org/10.1016/J.COMPOSITESA.2016.06.015

25. Dean, A., Sahraee, S., Reinoso, J., Rolfes, R.: A new invariant-based thermo-plastic model for finite deformation analysis of short fibre reinforced composites: Development and numerical aspects. Compos. Part B Eng. 125, 241–258 (2017). https://doi.org/10.1016/J.COMPOSITESB.2017.05.043

26. Dean, A., Grbic, N., Rolfes, R., Behrens, B.: Macro-mechanical modeling and experimental validation of

anisotropic, pressure- and temperature-dependent behavior of short fiber composites. Compos. Struct. 211, 630–643 (2019). https://doi.org/10.1016/J.COMPSTRUCT.2018.12.045

27. Behrens, B.A., Rolfes, R., Vucetic, M., Peshekhodov, I., Reinoso, J., Vogler, M., Grbic, N.: Material Characterization for FEA of the Clinching Process of Short Fiber Reinforced Thermoplastics with an Aluminum Sheet. Adv. Mater. Res. 966–967, 557–568 (2014). https://doi.org/10.4028/WWW.SCIENTIFIC.NET/AMR.966-967.557

28. Friedrich, K., Walter, R., Voss, H., Karger-Kocsis, J.: Effect of short fibre reinforcement on the fatigue crack propagation and fracture of PEEK-matrix composites. Composites. 17, 205–216 (1986). https://doi.org/10.1016/0010-4361(86)91004-9

29. Evans, W., Isaac, D., Saib, K.: The Effect of Short Carbon Fibre Reinforcement on Fatigue Crack Growth in PEEK. Composites. 27A, 547–554 (1996). https://doi.org/10.1016/1359-835X(96)00015-2

30. Brent Strong, A.: Fundamentals of Composites Manufacturing, Materials, Methods and Applications. Society of Manufacturing Engineers Dearborn, Michigan (2008)

31. Kim, H.G., Kwac, L.K.: Evaluation of elastic modulus for unidirectionally aligned short fiber composites. J. Mech. Sci. Technol. 23, 54–63 (2009). https://doi.org/10.1007/s12206-008-0810-1

32. Tucker, C.L., Liang, E.: Stiffness predictions for unidirectional short-fiber composites.pdf. Compos. Sci. Technol. 59, 655–671 (1999)

33. Sanomura, Y., Kawamura, M.: Fiber Orientation Control of Short-Fiber Reinforced Thermoplastics by Ram Extrusion. Polym. Compos. 24, 587–596 (2003). https://doi.org/10.1002/pc.10055

34. Junaedi, H., Baig, M., Dawood, A., Albahkali, E., Almajid, A.: Mechanical and physical properties of short carbon fiber and nanofiller-reinforced polypropylene hybrid nanocomposites. Polymers (Basel). 12, 1–25 (2020). https://doi.org/10.3390/polym12122851

35. Chen, F., Ou, H., Gatea, S., Long, H.: Hot tensile fracture characteristics and constitutive modelling of polyether-ether-ketone (PEEK). Polym. Test. 63, 168–179 (2017). https://doi.org/10.1016/j.polymertesting.2017.07.032

36. Pascual-González, C., Iragi, M., Fernández, A., Fernández-Blázquez, J.P., Aretxabaleta, L., Lopes, C.S.:

An approach to analyse the factors behind the micromechanical response of 3D-printed composites. Compos. Part B Eng. 186, 107820 (2020). https://doi.org/10.1016/j.compositesb.2020.107820

37. Mortazavian, S., Fatemi, A.: Effects of fiber orientation and anisotropy on tensile strength and elastic modulus of short fiber reinforced polymer composites. Compos. Part B Eng. 72, 116–129 (2015). https://doi.org/10.1016/j.compositesb.2014.11.041

38. Avanzini, A.: Effect of cyclic strain on the mechanical behavior of virgin ultra-high molecular weight polyethylene. J. Mech. Behav. Biomed. Mater. 4, 1242–1256 (2011). https://doi.org/10.1016/j.jmbbm.2011.04.010

39. Lemaitre, J.: A continuous damage mechanics model for ductile fracture. J. Eng. Mater. Technol. Trans. ASME. 107, 83–89 (1985). https://doi.org/10.1115/1.3225775

40. Nouri, H., Meraghni, F., Lory, P.: Fatigue damage model for injection-molded short glass fibre reinforced thermoplastics. Int. J. Fatigue. 31, 934–942 (2009). https://doi.org/10.1016/j.ijfatigue.2008.10.002

41. Ralph I. Stephens, Ali Fatemi, Robert R. Stephens, H.O.F.: Metal Fatigue in Engineering, 2nd Edition. John Wiley & Sons, Ltd (2000)

42. Horst, J.J., Spoormaker, J.L.: Mechanisms of fatigue in short glass fiber reinforced polyamide 6. Polym. Eng. Sci. 36, 2718–2726 (1996). https://doi.org/10.1002/pen.10671

43. Zhou, Y., Mallick, P.K.: Fatigue performance of an injection-molded short E-glass fiber-reinforced polyamide 6,6. I. Effects of orientation, holes, and weld line. Polym. Compos. 27, 230–237 (2006). https://doi.org/10.1002/pc.20182

44. De Monte, M., Moosbrugger, E., Quaresimin, M.: Influence of temperature and thickness on the off-axis behaviour of short glass fibre reinforced polyamide 6.6 - Quasi-static loading. Compos. Part A Appl. Sci. Manuf. 41, 859–871 (2010). https://doi.org/10.1016/j.compositesa.2010.02.018

45. Guster, C., Pinter, G., Mösenbacher, A., Eichlseder, W.: Evaluation of a simulation process for fatigue life calculation of short fibre reinforced plastic components. Procedia Eng. 10, 2104–2109 (2011). https://doi.org/10.1016/j.proeng.2011.04.348

46. Mejri, M., Toubal, L., Cuillière, J.C., François, V.: Hygrothermal aging effects on mechanical and fatigue behaviors of a short- natural-fiber-reinforced composite. Int. J. Fatigue. 108, 96–108 (2018). https://doi.org/10.1016/j.ijfatigue.2017.11.004